

Tellurium Analogues of Rosamine and Rhodamine Dyes: Synthesis, Structure, ^{125}Te NMR, and Heteroatom Contributions to Excitation Energies

Brandon Calitree, David J. Donnelly, Jason J. Holt, Michael K. Gannon, Cara L. Nygren, Dinesh K. Sukumaran, Jochen Autschbach,* and Michael R. Detty*

Department of Chemistry, University at Buffalo, The State University of New York, Buffalo, New York 14260-3000

Received August 22, 2007

The first tellurium-containing analogues of the rosamine and rhodamine dyes were prepared by the addition of Grignard or organolithium reagents to telluroxanthone precursors. The ^{125}Te spectra of both the dyes and the telluroxanthone precursors are reported. One derivative was characterized by X-ray crystallography and was found to have a nearly planar telluroxanthylum core with a 9-aryl substituent held nearly orthogonal to the core. Density functional theory (DFT) and time-dependent DFT (TDDFT) calculations were performed to analyze the trends for the excitation wavelengths observed experimentally. The computations indicated that participation of the heteroatom lone pair orbitals is responsible for this trend.

Introduction

The rhodamine and rosamine dyes are xanthylium chromophores that are useful as laser dyes, fluorescent labels, and fluorescence emission standards where their high fluorescence quantum yields and photostability can be exploited.¹ These chromophores typically have very low triplet yields (under 10%), which has limited studies of these molecules to their singlet state properties. Furthermore, classic rhodamine and rosamine chromophores have absorption maxima, λ_{max} , of less than 600 nm, which limits their utility in biological systems. Biosensing applications with these chromophores have used FRET² and electrochemiluminescence³ to populate the excited singlet state via energy transfer as well as by direct excitation. The rhodamines have also been described as sensors for protons⁴ and for halide salts⁵ through quenching of the singlet excited state. Because the rhodamine and rosamine derivatives have $\lambda_{\text{max}} < 600$ nm, their fluorescence sensitivity in biological systems is limited because they emit at the same wavelengths as the background biological autofluorescence from serum, proteins, and other macromolecular molecules.^{1e} Longer-wavelength-absorbing rhodamine and rosamine derivatives would emit at longer wavelengths, minimizing background contributions from

biofluid and tissue auto fluorescence. If one could control the photophysics of the rhodamine and rosamine chromophores to populate the triplet excited state via increased quantum yields for intersystem crossing, then longer-lived phosphorescence could be used as the sensing signal that could (a) be detected at longer wavelengths and (b) be detected long after background fluorescence had decayed away.

Several rhodamines and rosamines localize preferentially in selected biological sites.⁶ While fluorescence from the localized dyes can be used in imaging applications, the rhodamines and rosamines have not shown phototoxicity toward cancer cells, bacterial pathogens, or viral pathogens due to poor triplet yields.⁷ Brominated rhodamines⁸ and related compounds⁹ have been prepared that have increased quantum yields for the generation of singlet oxygen [$\Phi(^1\text{O}_2)$] due to the heavy-atom effect from the bromine atoms, but these derivatives also absorb with $\lambda_{\text{max}} < 600$ nm, which is outside the 600–900 nm window for optimal penetration of light in biological tissue. Consequently, these rhodamine analogues can only be used in ex vivo applications. If one could control the photophysics of the rhodamine and rosamine chromophores (a) to absorb at longer wavelengths and (b) to populate the triplet excited state, then rhodamine and rosamine chromophores could be used as photosensitizers in biological applications.¹⁰

* To whom correspondence should be addressed. Phone: (716) 645-6800. Fax: (716) 645-6963. E-mail: jochena@nsm.buffalo.edu (J.A.); mdetty@buffalo.edu (M.R.D.).

(1) (a) Peterson, O. G.; Tuccio, S. A.; Snavely, B. B. *Appl. Phys. Lett.* **1970**, *17*, 245–247. (b) Drexhage, K. H. *Laser Dyes, Top. Appl. Phys.* **1973**, *1*, 144–274. (c) Karstens, T.; Kobs, K. *J. Phys. Chem.* **1980**, *84*, 1871–1872. (d) Preininger, C.; Mohr, G. J.; Klimant, I.; Wolfbeis, O. S. *Anal. Chim. Acta* **1996**, *334*, 113–123. (e) Liu, J.; Diwu, Z.; Leung, W.-Y.; Lu, Y.; Patch, B.; Hugland, R. P. *Tetrahedron Lett.* **2003**, *44*, 4355–4359.

(2) (a) Adams, S. R.; Harootounian, A. T.; Buechler, Y. J.; Taylos, S. S.; Tsien, R. Y. *Nature* **1991**, *349*, 694–697. (b) Martinez-Manez, R.; Sancenon, F. *Chem. Rev.* **2003**, *103*, 4419–4476.

(3) Richter, M. M. *Chem. Rev.* **2004**, *104*, 3003–3036.

(4) (a) de Silva, A. P.; Gunaratne, H. Q. N.; Gunnaugsson, T.; Huxley, A. J. M.; McCoy, C. P.; Rademacher, J. T.; Rice, T. E. *Chem. Rev.* **1997**, *97*, 1515–1566. (b) Vogel, M.; Rettig, W.; Sens, D.; Drexhage, K. H. *Chem. Phys. Lett.* **1988**, *147*, 452–460.

(5) Anzenbacher, P., Jr.; Jursikova, K.; Sessler, J. L. *J. Am. Chem. Soc.* **2000**, *122*, 9350–9351.

(6) (a) Johnson, L. V.; Walsh, M. L.; Bockus, B. J.; Chen, L. B. *J. Cell Biol.* **1981**, *88*, 526–535. (b) Davis, S.; Weiss, M. J.; Wong, J. R.; Lampidis, T. J.; Chen, L. B. *J. Biol. Chem.* **1985**, *260*, 13844–13850.

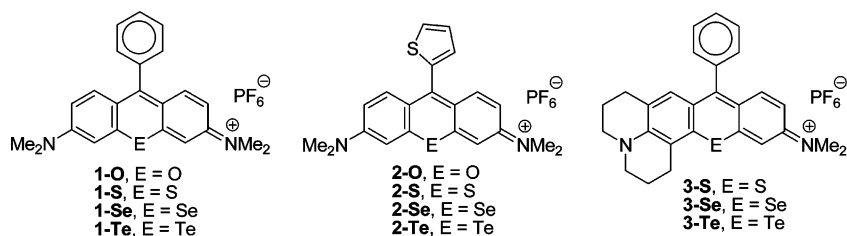
(7) Bernal, S. D.; Lampidis, T. J.; McIsaac, R. M.; Chen, L. B. *Science* **1986**, *222*, 169–172.

(8) (a) Brasseur, N.; Menard, I.; Forget, A.; El Jastimi, R.; Hamel, R.; Molfino, N. A.; van Lier, J. E. *Photochem. Photobiol.* **2000**, *72*, 780–787. (b) Pal, P.; Zeng, H.; Durocher, G.; Girard, D.; Li, T. C.; Gupta, A. K.; Giasson, R.; Blanchard, L.; Gaboury, L.; Balassy, A.; Turmel, C.; Laperriere, A.; Villeneuve, L. *Photochem. Photobiol.* **1996**, *53*, 161–168.

(9) (a) Shi, J.; Zhang, X.; Neckers, D. C. *J. Org. Chem.* **1992**, *57*, 4418–4421. (b) Parker, C. A. In *Advances in Photochemistry*; Noyes, W. A., Jr., Hammond, G. S., Pitts, J. N., Jr., Eds.; Wiley-Interscience: New York, 1964; Vol. 2, p 305.

(10) Detty, M. R.; Gibson, S. L.; Wagner, S. *J. Med. Chem.* **2004**, *47*, 3897–3915.

Chart 1. Tetramethylrosamine (1-O), Its Heavier Chalcogen Analogues, and Related Compounds



Rhodamine derivatives with longer wavelengths of absorption have been prepared by making derivatives that prevent rotation of the amino substituents on the xanthylum core.^{1e,11,12} However, these approaches do not increase triplet yields even though values of λ_{\max} may be > 600 nm. We have described a different approach to longer-wavelength-absorbing analogues of tetramethylrosamine (**1-O**, Chart 1) via substitution of the heavier chalcogen atoms S and Se for the O atom of the xanthylum chromophore (**1-S** and **1-Se**, respectively, Chart 1).¹³ In this series, values of λ_{\max} increase from 550 nm for **1-O** to 581 nm for **1-Se**, quantum yields for fluorescence, Φ_F , decreased 100-fold from 0.84 for **1-O** to 0.009 for **1-Se**, and values for the triplet yield, Φ_T , increased more than 10-fold from 0.08 for **1-O** to 0.97 for **1-Se**. Replacing the 9-phenyl substituent with a 9-(2-thienyl) group gave **2-S** and **2-Se** with roughly 20 nm longer values of λ_{\max} than **1-S** and **1-Se**, respectively, with λ_{\max} for **2-Se** of 601 nm.¹⁴ Constraining the rotation of one amino substituent in **3-S** and **3-Se** gave values of λ_{\max} roughly 10 nm longer than λ_{\max} for **1-S** and **1-Se**, respectively, with λ_{\max} of 581 nm for **3-S** and 588 nm for **3-Se**.¹⁵

The telluroxanthylum analogues **1-Te**, **2-Te**, and **3-Te** should absorb at longer wavelengths than the corresponding selenium analogues and have photophysics dominated by the triplet. However, these analogues are absent in earlier work because synthetic studies toward telluroxanthone precursors, using directed metalation to close the xanthone ring, suggested that the Te–C bond might be susceptible to Te–Li exchange.¹⁶ Synthetic routes to the telluroxanthone precursors using Friedel–Crafts-related chemistry have recently become available.¹⁷

It is apparent that the heteroatom contributes significantly to the observed physical and photophysical properties of the corresponding chalcogenoxanthylum dyes, and it would be highly desirable to reconcile the experimental parameters with those predicted from theory to quantify the contribution of the heteroatom to the chromophore. Time-dependent density functional theory (TDDFT) has been utilized to predict the electronic spectra of a variety of organic dyes and chromophores.^{18,19} In particular, TDDFT has worked well with chromophores containing the heteroatoms N and S,¹⁹ which suggests that similar

calculations with the chalcogenoxanthylum dye series such as **1-E** and **2-E** (E = O, S, Se, Te) will be accurate for the heavier chalcogen analogues bearing Se and Te.

Herein, we describe the synthesis of the first tellurorosamine and tellurorhodamine analogues from telluroxanthone precursors. The Te–C bond is stable to the conditions of reaction, and the tellurorosamines and rhodamines are stable, crystalline compounds permitting the structure of **1-Te** to be determined by X-ray crystallographic analysis. The experimental electronic absorption spectra for the dye series **1-E** and **2-E** were compared to those predicted by TDDFT. All of the telluroxanthylum dyes prepared in this study have values of λ_{\max} near 600 nm or longer wavelengths.

Results and Discussion

Synthesis of Tellurorosamine and Tellurorhodamine Dyes.

The telluroxanthone **4-Te**^{17a} served as a useful precursor to the tellurorosamine and rhodamine dyes as shown in Scheme 1. The addition of a THF solution of PhMgBr to **4-Te** followed by the addition of aqueous 10% HPF₆ gave tellurorosamine **1-Te** in 78% isolated yield. There was no indication of cleavage of the Te–C bond, and the only byproduct was a 7% recovered yield of telluroxanthone **4-Te**. Tellurorosamine **1-Te** had λ_{\max} of 601 nm in CH₂Cl₂ and 597 nm in H₂O or MeOH.

The Te–C bond was also stable to the addition of organolithium reagents to the telluroxanthone carbonyl group (Scheme 1). A solution of 2-lithiothiophene was added to telluroxanthone **4-Te** at -78 °C followed by quenching with aqueous HPF₆. The telluroxanthylum dye **2-Te** was isolated in 59% yield following recrystallization from CH₃CN/ether. The addition of 1-lithionaphthalene, prepared via lithium–halogen exchange between 1-bromonaphthalene and *sec*-BuLi, to telluroxanthone **4-Te** gave 9-(1-naphthyl)telluroxanthylum dye **5-Te** in 59% isolated yield following quenching with aqueous HPF₆.

Both **2-Te** and **5-Te** had longer-wavelength values of λ_{\max} relative to **1-Se**. For **2-Te**, λ_{\max} was 615 nm in CH₂Cl₂, 611 nm in H₂O, and 615 nm in MeOH. Values of λ_{\max} for **5-Te** were 602 nm in CH₂Cl₂ and 604 nm in H₂O.

The Te–C bond was also stable to more reactive organolithium agents. The addition of 2 equiv of *tert*-BuLi to 5-bromothiophene-2-carboxylic acid in the presence of 0.5 equiv of TMEDA gave lithium 5-lithiothiophene-5-carboxylate (**6**).²⁰ The addition of **6** to telluroxanthone **4-Te** followed by quenching with aqueous HPF₆ gave 9-(5-carboxylato-2-thienyl)telluroxanthylum dye **7-Te** in 46% isolated yield (Scheme 1).

Bromine–lithium exchange in 2-bromobenzoic acids has been utilized to generate lithium 2-lithiobenzoate (**8**).²¹ While the

(11) Sauer, M.; Han, K.-T.; Muller, R.; Nord, S.; Schulz, A.; Seeger, S.; Wolfrum, J.; Arden-Jacob, J.; Deltau, G.; Marx, N. J.; Zander, C.; Drexhage, K. H. *J. Fluoresc.* **1995**, *5*, 247–261.

(12) Haugland, R. P. *Handbook of Fluorescent Probes and Research Products*, 9th ed.; Molecular Probes, Inc.: Eugene, OR, 2002.

(13) Ohulchanskyy, T.; Donnelly, D. J.; Detty, M. R.; Prasad, P. N. *J. Phys. Chem. B* **2004**, *108*, 8668–8672.

(14) Wagner, S. J.; Skripchenko, A.; Donnelly, D. J.; Ramaswamy, K.; Detty, M. R. *Biorg. Med. Chem.* **2005**, *13*, 5927–5935.

(15) Holt, J. J.; Gannon, M. K.; Tomblin, G.; McCarty, T. A.; Page, P. M.; Bright, F. V.; Detty, M. R. *Biorg. Med. Chem.* **2006**, *14*, 8635–8643.

(16) Brennan, N. K.; Donnelly, D. J.; Detty, M. R. *J. Org. Chem.* **2003**, *68*, 3344–3347.

(17) (a) Del Valle, D. J.; Donnelly, D. J.; Holt, J. J.; Detty, M. R. *Organometallics* **2005**, *24*, 3807–3810. (b) Holt, J. J.; Calitree, B. D.; Vincek, J.; Gannon, M. K., II; Detty, M. R. *J. Org. Chem.* **2007**, *72*, 2690–2693.

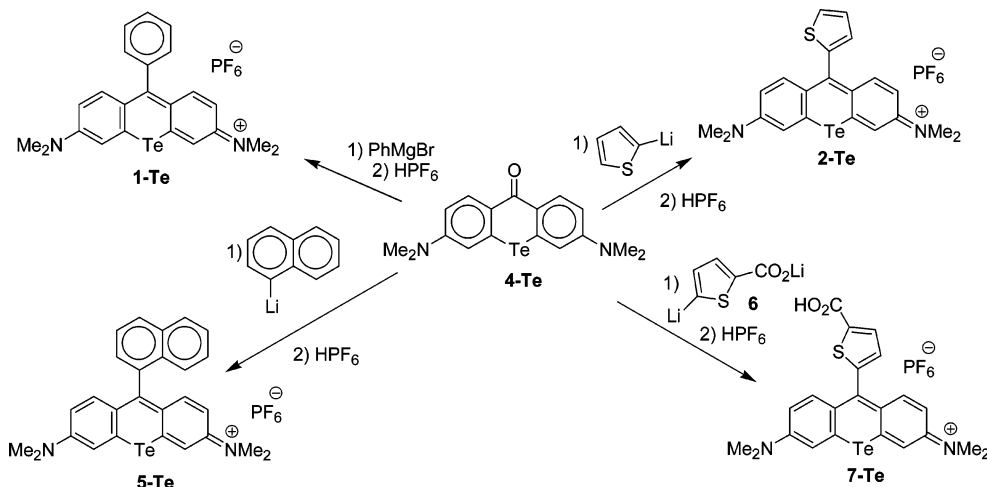
(18) (a) Sheikhshoia, I.; Fabian, W. M. F. *Dyes Pigm.* **2005**, *70*, 91–98. (b) Guillaumont, D.; Nakamura, S. *Dyes Pigm.* **2000**, *46*, 85–92.

(19) (a) Coe, B. J.; Beljonne, D.; Vogel, H.; Garin, J.; Orduna, J. *J. Phys. Chem. A* **2005**, *109*, 10052–10057. (b) Fabian, J.; Diaz, L. A.; Seifert, G.; Niehaus, T. *THEOCHEM* **2002**, *594*, 41–53. (c) Andreu, R.; Garin, J.; Orduna, J. *Tetrahedron* **2001**, *57*, 7883–7892.

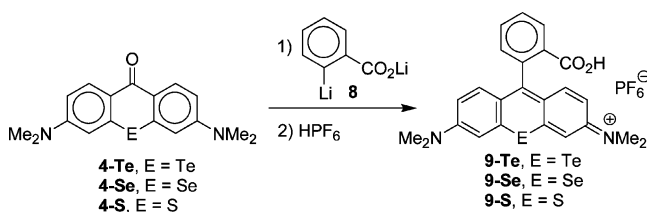
(20) Gannon, M. K., II; Detty, M. R. *J. Org. Chem.* **2007**, *72*, 2647–2650.

(21) (a) Parham, W. E.; Sayed, Y. A. *J. Org. Chem.* **1974**, *39*, 2051. (b) Parham, W. E.; Sayed, Y. A. *J. Org. Chem.* **1974**, *39*, 2053.

Scheme 1. Synthesis of Tellurosamine and Tellurorhodamine Derivatives



Scheme 2. Preparation of Chalcogenorhodamine Derivatives 9-E via the Addition of Lithium 2-Lithiobenzoate (8)



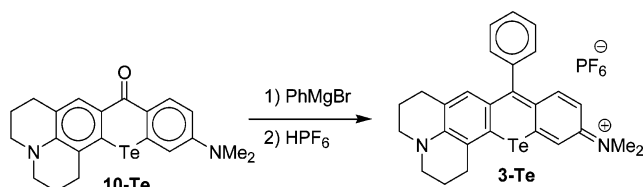
dianion **8** is stable at $-75\text{ }^{\circ}\text{C}$ or colder, warmer temperatures result in self-addition reactions to form benzoylbenzoic acid products.²¹ Treating benzoic acid at $-90\text{ }^{\circ}\text{C}$ with 2.2 equiv of a 1:1 mixture of *sec*-BuLi/TMEDA in tetrahydrofuran (THF) also generates dianion **8**, which reacts with a variety of electrophiles to give 2-substituted benzoic acids.²² Unfortunately, the addition of **8** generated via either method to telluroxanthone **4-Te** at $-78\text{ }^{\circ}\text{C}$ was sluggish and generated very little of the desired product ($<5\%$).

The addition of 2.1 equiv²⁰ (not 3.1 equiv, which includes the customary 2 equiv of *tert*-BuLi for lithium–bromine exchange) of *tert*-BuLi to 2-bromobenzoic acid and 0.25 equiv of TMEDA (relative to 2-bromobenzoic acid) in anhydrous THF at $-78\text{ }^{\circ}\text{C}$ generated the dianion **8**. A 4-fold excess of **8** from this mixture was then added to a solution of **4-Te** in THF at ambient temperature. The resulting mixture was then heated at reflux for 15 min followed by quenching with $\text{CH}_3\text{CO}_2\text{H}$ and then HPF_6 . Dye **9-Te** as the carboxylic acid was isolated in 89% yield following recrystallization of the crude product. Similar results were obtained with chalcogenoxanthones **4-Se** and **4-S** where the acids **9-Se** and **9-S** were isolated in 84% and 75% yields, respectively, following recrystallization (Scheme 2). Tellurorhodamine **9-Te** has λ_{max} of 601 nm in CH_2Cl_2 and 595 nm in H_2O , while chalcogenorhodamines **9-Se** and **9-S** have values of λ_{max} of 580 and 572 nm, respectively, in H_2O .

The addition of PhMgBr to telluroxanthone derivative **10-Te**^{17b} gave telluroxanthylum dye **3-Te** in 89% isolated yield following the addition of aqueous 10% HPF_6 to the reaction mixture (Scheme 3). Tellurosamine **3-Te** has λ_{max} of 605 nm in CH_2Cl_2 and 604 nm in MeOH.

X-ray Crystal Structure of Tellurotetramethylrosamine (1-Te). Crystals of **1-Te** suitable for X-ray crystallographic

Scheme 3. Preparation of Chalcogenosamine Derivatives 3-Te



analysis were prepared via recrystallization of **1-Te** from 1:1 $\text{CH}_3\text{CN}/\text{ether}$. ORTEP drawings of the crystal structure of **1-Te** at the 50% probability level are shown in Figure 1 viewed (a) from the top and (b) along the Te1–C7 axis. The molecule in the crystalline form is nearly planar with a slight 5° twist to the molecule. Crystal structures of **1-S** and **1-Se** as the bromide salts have been reported.²³ Both **1-S** and **1-Se** are nearly planar, as well, with approximately 3° of twist. Steric interactions between the *peri*-hydrogens of the xanthylium ring and the *ortho*-hydrogens of the 9-phenyl substituent force the phenyl substituent to be out of the plane of the xanthylium core. The dihedral angles for these relationships in the various crystals are 68.9° for **1-S**, 86.9° for **1-Se**, and 69.0° for **1-Te**. The central ring of **1-Te** is distorted by the long (2.07 Å) Te–C bonds and the 95.3° Te–C bond angle. The dimethylamino substituents at the 2- and 7-positions of **1-Te** are also coplanar with the xanthylium core with considerable double-bond character to the C–N bonds to the ring (1.34–1.35 Å).

Crystal structures for both rhodamine **6G** (**R6G**) and rhodamine 123 (**Rh-123**) have been described.²⁴ In both molecules, the xanthylium core is planar and the 9-aryl substituent is nearly orthogonal to the plane with dihedral angles of 63.3° for **R6G** and 88.0° for **Rh-123**. Table 1 contains a summary of structural information for **R6G**, **Rh-123**, **1-S**, **1-Se**, and **1-Te**.

As the chalcogen atom increases in size, the C–E bond length increases from 1.37–1.38 Å for the C–O bond lengths to 2.07 Å for the C–Te bond length. With this change, the central ring is distorted as the C–E–C angle decreases from 120° for **R6G** and **Rh-123** to 95.3° for **1-Te** and the $\text{N}\cdots\text{E}\cdots\text{N}$ angle decreases from 180° for the rhodamine derivatives to 153.27° for **1-Te**. Interestingly, the changes in C–E bond lengths have little impact on the $\text{N}\cdots\text{N}$ distances in this series. For **R6G** and **Rh-123**, the

(23) Tomblin, G.; Donnelly, D. J.; Holt, J. J.; You, Y.; Ye, M.; Gannon, M. K.; Nygren, C. L.; Detty, M. R. *Biochemistry* **2006**, *45*, 8034–8047.

(24) Adhikesavalu, D. N.; Mastropaolo, D.; Camerman, A.; Camerman, N. *Acta Crystallogr., Sect. C* **2001**, *57*, 657–659.

(22) Mortier, J.; Moyroud, J.; Bennetau, B.; Cain, P. A. *J. Org. Chem.* **1994**, *59*, 4042.

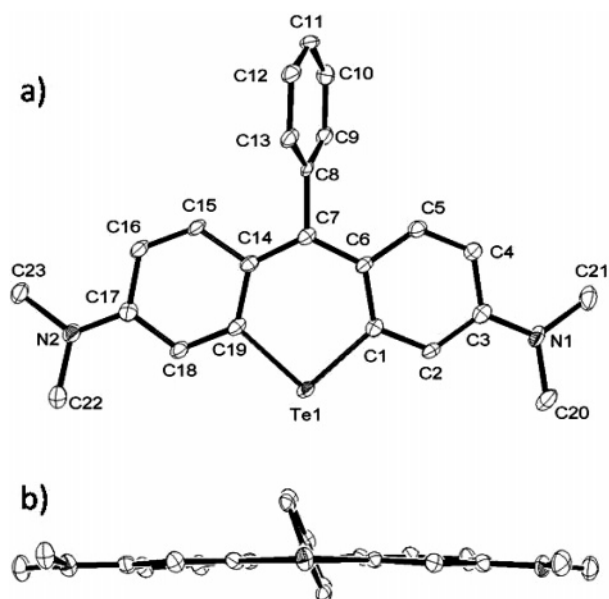


Figure 1. ORTEP plot and label scheme for **1-Te**. Displacement ellipsoids are drawn at the 50% probability level viewed (a) from the top and (b) edge on down the Te1–C7 axis. Hydrogen atoms and the PF₆ anion are omitted for clarity.

Table 1. Comparative C–E Bond Lengths, N···E and N···N Distances, and 9-Aryl-xanthylum Dihedral Angles for R6G, Rh-123, 1-S, 1-Se, and 1-Te

compd	C–E bond length, Å	N···E distance, Å	N···N distance, Å	9-aryl-xanthylum dihedral, deg
R6G ^a	1.37	5.0	10.0	63.3
Rh-123 ^a	1.38	5.0	10.0	88.0
1-S ^b	1.73	5.04	10.007	68.9
1-Se ^b	1.88	5.13	10.155	86.9
1-Te	2.07	5.27	10.292	69.0

^a Data from ref 24. ^b Data from ref 23.

N···N distance is roughly 10.0 Å.²⁴ The N···N distance increases only to 10.29 Å in **1-Te**.

The X-ray structural data for **R6G**, **Rh-123**, **1-S**, **1-Se**, and **1-Te** provide a starting point for geometry optimization in the theoretical studies described below. In all of these molecules, the planarity of the xanthylum core has implications for the effectiveness of overlap of AO's on the chalcogen atom with the adjacent carbon π -framework.

¹²⁵Te NMR Spectra of Telluroxanthenes and Telluroxanthylum Dyes. The positive charge on the rosamine and rhodamine structures will impact the charge density on the chalcogen atom both through delocalization with the adjacent carbon π -framework as well as through purely inductive effects. The ¹²⁵Te NMR spectra of the telluroxanthylum dyes should give some indication of the effect of substituents on the electron density at the tellurium atom. ¹²⁵Te NMR data are compiled in Table 2 for the telluroxanthylum dyes of this study as well as for the telluroxanthenes **4-Te** and **10-Te** and for the parent telluroxanthone **11**.^{25,26}

The ¹²⁵Te NMR spectra for **1-Te**, **2-Te**, **4-Te**, and **5-Te** (Supporting Information) are triplets with strong coupling (29–31 Hz) to two protons. The ¹²⁵Te NMR spectra for **3-Te** and **10-Te** (Supporting Information) are doublets with coupling constants of 34 and 33 Hz, respectively. These observations

are consistent with ³J coupling between the Te atom and the two protons at C1 and C8 for **1-Te**, **2-Te**, **4-Te**, and **5-Te** and the single proton at C8 for **3-Te** and **10-Te**. This assignment was made unambiguously following the proton decoupling illustrated in Figure 2. Here, decoupling of either the H_A or the H_B proton had no impact on the multiplicity of the signal. However, decoupling of H_C collapsed the triplet to a singlet, confirming the nature of the large ³J_{Te–H} coupling observed in the experimental spectra.

The reported chemical shifts for the parent telluroxanthone **11** are δ 473.4²⁵ and δ 471.5.²⁶ Telluroxanthone **11** can place positive charge on the Te atom through resonance form **I** (Chart 2). Telluroxanthenes **4-Te** and **10-Te** can also place positive charge on the Te atom via resonance form **II**, but the amino substituents at the 2- and 7-positions can also localize the charge through resonance forms **III**, which diminishes the net charge at Te. Consequently, both **4-Te** and **10-Te** have ¹²⁵Te chemical shifts that are upfield of the shift for **11** at δ 442.2 and δ 329.9, respectively. In **10-Te**, the julolidyl amino group is locked into conjugation with the carbon π -framework, which would place even more positive charge at the N atom and contribute to the upfield shift of the ¹²⁵Te NMR signal for **10-Te**.

The contributions from conformational locking are also apparent in a comparison of the ¹²⁵Te chemical shifts for the telluroxanthylum dyes **1-Te** and **3-Te**, where the shift for **3-Te** is 114 ppm upfield of that for **1-Te**. The upfield shift is identical in comparing **4-Te** to **10-Te** and **1-Te** to **3-Te**. The ¹²⁵Te chemical shifts for all of the telluroxanthylum dyes are >230 ppm downfield from their telluroxanthone precursors, which reflects the formal positive charge in the telluroxanthylum dyes. In these systems, the positive charge can be placed on the Te atom via resonance forms related to **IV** (Chart 2) or on the 2,7-amino substituents via resonance forms **V**.

Excitation Energies from ab Initio Computational Methods. To analyze the heteroatom contributions to the trend seen in the excitation energies of the chalcogenorhodamine and rosamine dyes, the dye series **1-E** and **2-E** (E = O, S, Se, Te) were examined with the help of density functional theory (DFT) and time-dependent DFT (TDDFT)^{27,28} calculations using the methods described in the computational section of the Experimental Section. Table 3 lists the computed vertical excitation energies for the excited singlet state for all eight compounds using the B3LYP/TZVP level of theory²⁹ and compares them to the wavelengths of the absorption maxima. The energies are the ones for the lowest energy excited states, characterized in the TDDFT computations as HOMO–LUMO $n-\pi^*$ transitions. (Orbital visualizations of the HOMO and LUMO are found in Figures 1S and 2S, Supporting Information.) It can be seen that there is a consistent overestimation of the excitation energies relative to the experimental values. Without considering solvent effects in the computations the overestimations range is from 0.75 to 0.82 eV, which corresponds to an underestimation in wavelength from 148 to 168 nm. The addition of solvent, polar or nonpolar, has little effect, with reduced ranges of 0.73–0.79 eV and corresponding wavelength underestimation of 126–144 nm. The systematic overestimation of the calculated excitation energies is consistent with previously reported findings for

(27) Casida, M. E. Time-dependent density functional response theory for molecules. In *Recent advances in density functional methods*; Chong, D. P., Ed.; World Scientific: Singapore, 1995; Vol. 1, pp 155–192.

(28) Bauernschmitt, R.; Ahlrichs, R. *Chem. Phys. Lett.* **1996**, *256*, 454–464.

(29) Ahlrichs, R.; Bar, M.; Haser, M.; Horn, H.; Kolmel, C. *Chem. Phys. Lett.* **1989**, *162*, 165.

(25) Levy, A.; Biedermann, R. U.; Cohen, S.; Agrat, I. *Phosphorus, Sulfur Silicon Relat. Elem.* **1998**, *136–138*, 139–142.

(26) Nakanishi, W.; Yamamoto, Y.; Hayashi, S.; Tukada, H.; Iwamura, H. *J. Phys. Org. Chem.* **1990**, *3*, 369–374.

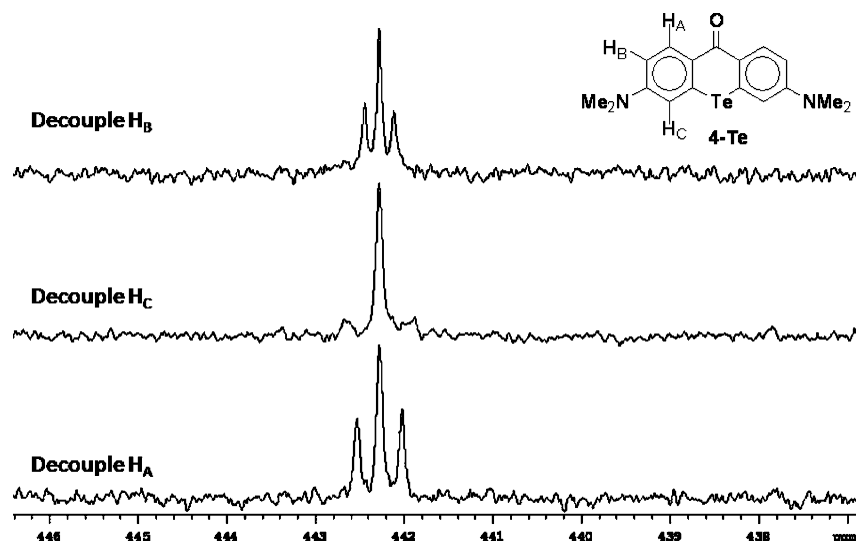
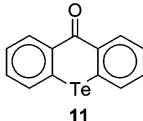
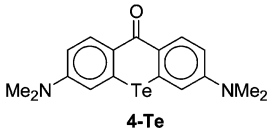
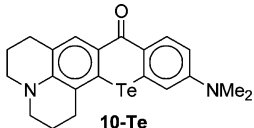
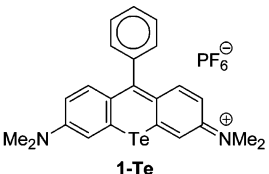
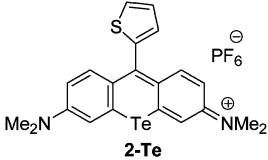
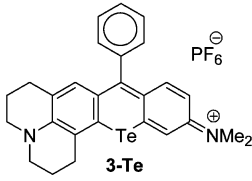
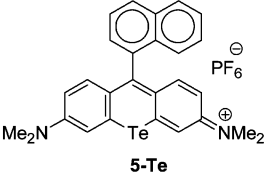


Figure 2. ^{125}Te NMR spectra of telluroxanthone **4-Te** with selective proton decoupling. Top spectrum, with H_B decoupled (δ 6.70). Middle spectrum, with H_C decoupled (δ 6.76). Bottom spectrum, with H_A decoupled (δ 8.53).

Table 2. ^{125}Te NMR Chemical Shifts and $^3J_{\text{Te-H}}$ Coupling Constants for Telluroxanthylum Dyes **1-Te**, **2-Te**, **3-Te**, and **5-Te** and Telluroxanthenes **4-Te**, **10-Te**, and **11**

	^{125}Te NMR, δ ($^3J_{\text{Te-H}}$) ^a	^{125}Te NMR, δ ($^3J_{\text{Te-H}}$) ^a
	473.4 ^b 471.5 ^c	
	442.2 (33 Hz)	
	329.9 (33 Hz)	
	676.2 (29 Hz)	
		701.6 (31 Hz)
		562.8 (34 Hz)
		696.0 (31 Hz)

^a Relative to δ $^{125}\text{TeMe}_2 = 0.0$. ^b Reference 25. ^c Reference 26.

molecules with similar chromophores.³⁰ At present, it is unclear what is the exact origin of this systematic deviation, but it is safe to assume that the approximations in the density functional and the exchange-correlation kernel play a role. On the positive side, and more importantly, the computations reproduce the experimental trend of decreasing excitation energy along the series E = O, S, Se, Te quite well. When the computed data are compared to experimental energies, there is a linear trend with a correlation reasonably close to 1 ($R^2 > 0.98$, Figure 3). However, it is seen that the slope is greater than 1.0, which is indicative that there is also an overestimation of the magnitude of this trend in addition to the overestimation of the excitation energies themselves.

The dyes were also examined using the B3LYP (Figure 3S, Supporting Information) and the BLYP functionals (Figure 4S, Supporting Information), which both contain less of an exact exchange contribution than B3LYP. Both the B3LYP (20% exact exchange) and the BLYP (no exact exchange) functionals yielded excitation energies that were closer to the experimental values. However, both functionals led to a poorer correlation between theoretical and experimental excitation energies ($R^2 < 0.92$ for B3LYP and $R^2 < 0.86$ for BLYP) and afforded an even more positive slope than the B3LYP functional. It appears that, unlike for some other classes of molecules, the exact exchange contribution in the functional cannot simply be tuned to reduce the systematic overestimation of the calculated excitation energies and improve the slope and overall quality of the correlation between theory and experiment simulta-

(30) Champagne, B.; Guillaume, M.; Zutterman, F. *Chem. Phys. Lett.* **2006**, 425, 105.

Chart 2. Resonance Structures for Telluroxanthones and Telluroxanthylum Dyes

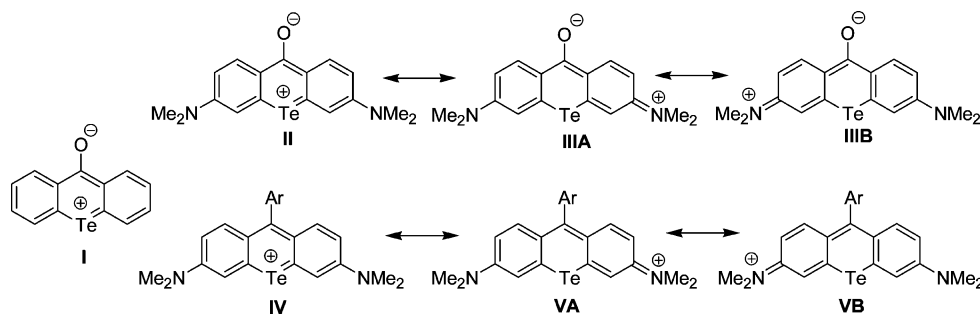


Table 3. Theoretical TDDFT and Experimental Excitation Energies

compound	theory (BHYLP)			experimental	
	vacuo	chloroform	methanol	ΔE , eV	λ , nm ^a
1-O	3.07	3.05	3.04	2.25	552
1-S	2.96	2.93	2.92	2.17	571
1-Se	2.91	2.88	2.87	2.13	582
1-Te	2.86	2.84	2.83	2.08	597
2-O	2.98	2.96	2.96	2.18	568
2-S	2.88	2.86	2.85	2.10	590
2-Se	2.83	2.80	2.79	2.06	601
2-Te	2.77	2.76	2.75	2.02	615

^a In MeOH.

neously. We have also investigated the influence of solvent effects in the computations. The results are shown in Figure 3. Although the calculated excitation energies are lowered when applying a solvent model for the ground state, the quality of the fit slightly deteriorates. In any case, the lowering of the excitation energies is not dramatic, and therefore ground-state solvation may be ruled out as one of the major sources of error in the computations. We decided to proceed with the analysis using the gas-phase BHYLP data. In summary, the overall reasonable correlation between theoretical and experimental data is sufficient for the purpose of this work to determine the origin of the trend for the excitation wavelengths along the E = O, S, Se, Te series.

To rationalize the change in excitation energies when we substitute S, Se, or Te for O, we examined the natural bond order (NBO) analysis for the dye series 1-E and 2-E. As shown in Chart 3, two different types of resonance systems exist within each chromophore that may contribute to the overall wavelength of absorption. One is the anthracene-like resonance forms typified by VI, and the other is cyanine dye-like resonance forms

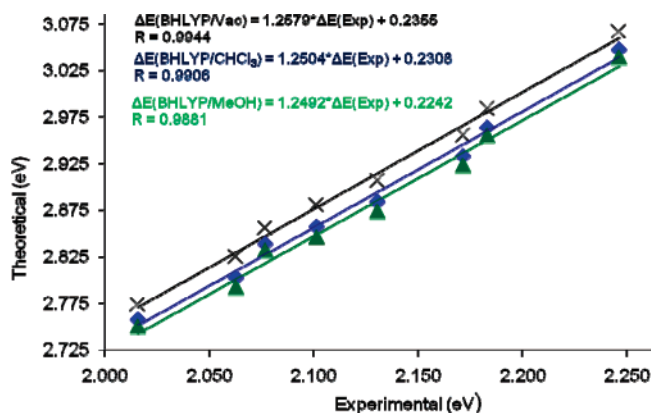
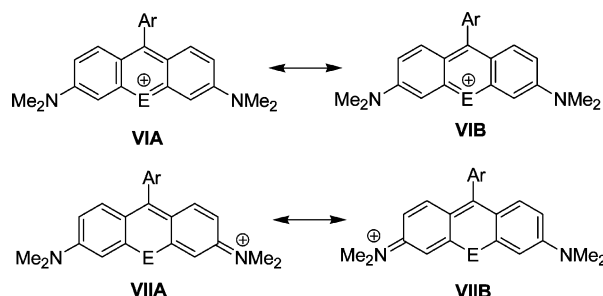


Figure 3. Theoretical versus experimental excitation energies. Solvent effects for the ground state treated with the COSMO continuum solvent model. Excitation energies calculated with the BHYLP functional and the TZVP basis set.

Chart 3. Anthracene-like (VIA and VIB) and Cyanine-like (VIIA and VIIIB) Resonance Forms in Chalcogenorhodamine dyes



as typified by VII. On the basis of which heteroatom is present in the compound, we consider a model where the “percentage” contribution from each resonance form and the amount of coupling between the different excitations vary. Each of the heteroatoms, O through Te, has the ability to donate charge from their lone pair orbitals into the π -system. As we shall show below, the amount of this charge donation correlates with the trends seen for the wavelengths of absorption.

In a C–C double bond, the p orbitals are identical and of the same size. If one of those C atoms were replaced with a larger atom such as S, the p–p orbital overlap would be diminished due to the increased size of the sulfur 3p orbital relative to the carbon 2p orbital and the resulting π -bond would be weaker. Therefore, the ability or likelihood that S would donate or share its p electrons in a S–C double bond would be less than that of the C–C double bond. In the xanthylum dye series, as the heteroatom increases in size, the heteroatom–carbon π -bond becomes weaker, therefore making the heteroatom donation of p electrons into the π -system less likely. Evidence for this may be obtained in an ab initio computation from an NBO (natural bond orbital) analysis by considering the occupation of the lone pair π -electrons of the heteroatom (Table 4).

From Table 4, lone pair 1 on O has a quite different hybridization (essentially sp^2) relative to S ($sp^{0.6}$), Se ($sp^{0.4}$), or Te ($sp^{0.3}$) in the series 1-E and 2-E where the hybridization between s and p orbitals is much less important, as evident from the computations. The increased s-character for the heavier chalcogen atoms in lone pair 1 reflects the increasing p_σ character in the σ bonds formed between the heavier chalcogen atoms S, Se, and Te and the two adjacent carbon atoms. While occupancy numbers are similar within the two series (a range of 1.673–1.701), the occupancy of lone pair 1 increases slightly as the chalcogen atom increases in size and the occupancy of lone pair 2 increases from S to Se to Te. However, the occupancy of lone pair 2 in both xanthylum analogues is greater than either the corresponding S- or Se-containing analogues. The second-order perturbation theory analysis carried out by the NBO code shows that the stabilization energy received

Table 4. Heteroatom Lone Pair Occupancy and Hybridization along with the Stabilization Energy Associated with Delocalizing These Electrons into the π -System of the Compound, According to the NBO Analysis

compd	atom	LP 1 occupancy	hybridization	energy, kcal mol ⁻¹	LP 2 occupancy	hybridization	energy, kcal mol ⁻¹
1-O	O	1.956	sp ^{2.2}	15.06	1.690	p	70.21
1-S	S	1.979	sp ^{0.6}	6.26	1.675	p	46.85
1-Se	Se	1.985	sp ^{0.4}	4.61	1.682	p	37.86
1-Te	Te	1.990	sp ^{0.3}	3.08	1.701	p	27.95
2-O	O	1.955	sp ^{2.2}	15.19	1.692	p	70.21
2-S	S	1.979	sp ^{0.6}	6.33	1.673	p	46.93
2-Se	Se	1.985	sp ^{0.4}	4.62	1.678	p	37.80
2-Te	Te	1.990	sp ^{0.3}	3.12	1.696	p	27.91

Table 5. TDDTF Excitation Energy and Ground-State NBO Analysis for the Optimized 1-Te and 2-Te Scaffolds with Heteroatom Replacement To Yield 1-Se(Te), 1-S(Te), 2-Se(Te), and 2-S(Te) (See Text for Details)

compd	ΔE , eV	λ , nm	atom	LP 1 occupancy	hybrid	energy, kcal mol ⁻¹	LP 2 occupancy	hybrid	energy, kcal mol ⁻¹
1-Te(S)	2.78	446	S	1.992	sp ^{0.2}	1.55	1.853	p	15.05
1-Te(Se)	2.81	441	Se	1.992	sp ^{0.2}	2.00	1.795	p	9.84
1-Te	2.86	434	Te	1.990	sp ^{0.3}	3.08	1.701	p	27.95
2-Te(S)	2.70	459	S	1.992	sp ^{0.2}	1.57	1.852	p	14.80
2-Te(Se)	2.73	454	Se	1.992	sp ^{0.2}	2.03	1.792	p	19.89
2-Te	2.77	448	Te	1.990	sp ^{0.3}	3.12	1.696	p	27.91

through the delocalization of the lone pair of electrons is consistent in that O will have the greatest effect when donating its electrons for resonance stabilization. These results are therefore consistent with chemical intuition.

Heteroatom lone pair occupancy and resonance stability are major determinants of the energetics of excitation because in our model these factors dictate the “percentages” of anthracene- and cyanine-like resonance forms that contribute to the overall excitation energies of each compound. We therefore propose the following rationale for the trend seen in the experiment for the absorption wavelength of **1-E** and **2-E**: When there is more “cyanine-type” resonance, it will result in a chromophore with a larger linear extension and, therefore, longer wavelengths of absorption. (This length-dependent trend can be explained, for example, by using a simple particle in a box model³¹ and is in agreement with the large body of experimental data for cyanines.) As the heteroatom donates/delocalizes its lone pair orbital, it disrupts the longer cyanine chromophore resulting in a π -system with a chromophore of shorter linear extension and, thus, shorter wavelengths of absorption. In consequence, one would expect the highest excitation energies/shortest excitation wavelengths for systems where the heteroatom participates most strongly in the π system (O, S), which is in agreement with the experimental data.

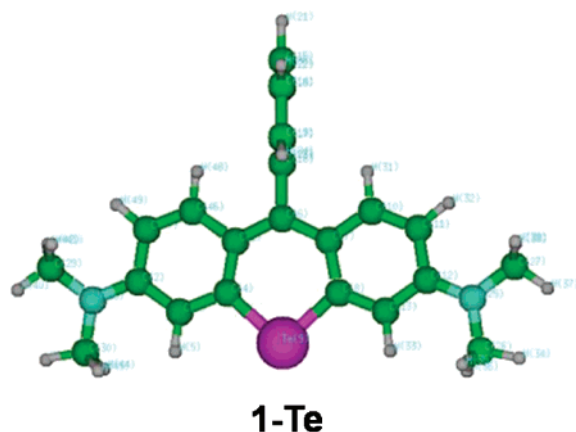
Another example of isolating the heteroatom contributions to resonance came as a consequence of taking the optimized

geometry for **1-Te** (Figure 4) and **2-Te** and replacing the Te atom with Se and S to give hybrid structures **1-Se(Te)** and **1-S(Te)**, respectively, with the geometry of **1-Te** and **2-Te** and rerunning the excitation-energy calculations (Table 5). Because of the longer heteroatom–carbon bond lengths, both the selenoxanthylum analogues and the thioxanthylum analogue exhibited a less effective delocalization of their lone pair electrons as compared to the optimized structures of **1-S/Se** and **2-S/Se**. This increased lone pair orbital occupancy goes along with a lower calculated energy for excitation and, therefore, longer wavelengths of absorbance, as expected (see Table 5). These calculations were initially carried out in an attempt to isolate the structural from electronic effects. The fact that a change of the heteroatom in the fixed geometry of the chromophore has an effect of a magnitude similar to that of the experimental trends for E = O, S, Se, Te strongly suggests that the influence of the heteroatom is predominantly a direct electronic effect (via participation in the π system) and not simply a trend caused by the somewhat different geometries of the chromophores due to the size of the heteroatom.

Summary and Conclusions

We have described the syntheses of the first telluroxanthylum analogues of the rosamines and rhodamines. These materials are stable, crystalline solids with strong absorbance at wavelengths ≥ 600 nm. X-ray crystallographic analysis of the structure of **1-Te** shows a nearly planar telluroxanthylum core with about 5° of twist. The 9-phenyl substituent is bent out of the plane of the telluroxanthylum core due to the interactions of the *ortho*-hydrogens of the phenyl group. Two interesting structural features among the rosamine/rhodamine dyes are that the N \cdots N distances vary little as the chalcogen atom increases in size (10.0–10.3 Å), while the N \cdots E \cdots N angle (E = O, S, Se, Te) decreases from 180° for the parent xanthylum structure to 153° in the telluroxanthylum dye **1-Te**. This is a consequence of the increased C–Te bond length (2.07 Å) and decreased C–Te–C bond angle (95.3°). In the optimized geometry for computational studies, the phenyl–telluroxanthylum dihedral angle is 90°.

The telluroxanthylum analogues of the rosamines and rhodamines absorb at longer wavelengths than their lighter

**Figure 4.** Optimized geometry for telluroxanthylum dye **1-Te**.(31) Kuhn, H. *J. Chem. Phys.* **1949**, *17*, 1198–1212.

chalcogen analogues. ^{125}Te NMR studies suggest that cyanine-like resonance is important in the delocalization of positive charge in these molecules, while computational studies indicate that anthracene-like resonance decreases as the chalcogen atom increases in size, due to poorer overlap of the heteroatom p-orbital with the carbon π -framework, and contributions from the longer cyanine-like resonance increase leading to longer wavelengths of absorbance and lower excitation energies. Using TDDFT/BHLYP/TZVP computations of the electronic spectra along with DFT-based analyses of the ground-state electronic structure, good correlation is observed between theoretical and experimental excitation energies, which can be rationalized on the basis of the heteroatom's capability to participate in the π system. We are currently investigating the photophysical properties of the telluroxanthylum dyes as well as various biological applications of these materials.

One potential concern in biological applications of the telluroxanthylum dyes is the toxicity associated with the Te atom. While we have not as yet conducted in vivo studies with these dyes, earlier studies with telluropyrylium dyes indicated that no toxicity was observed in three telluropyrylium analogues at doses between 5 and 11 mg/kg (7–19 $\mu\text{M}/\text{kg}$).³² Therapeutic doses of chalcogenopyrylium dyes and other cationic dyes have been on the order of 5–10 $\mu\text{mol}/\text{kg}$.³³ One would expect efficacy and toxicity similar to those of the telluropyrylium dyes.

Experimental Section

2,7-Bis(dimethylamino)-9-phenyltelluroxanthylum Hexafluorophosphate (1-Te). Phenylmagnesium bromide (1.0 M solution in THF, 1.0 mL, 1.0 mmol) was added to a stirred solution of 2,7-bis(dimethylamino)telluroxanthone-9-one (**4-Te**, 0.125 g, 0.32 mmol) in anhydrous THF (5 mL). The resulting solution was heated at reflux for 1 h. The reaction mixture was then cooled to ambient temperature and added slowly to 50 mL of 5% (by weight) HPF₆. The resulting mixture was cooled to $-10\text{ }^\circ\text{C}$ precipitating the dye **1-Te**. The dye was collected by filtration, and the solid was washed with water (2 \times 5 mL) and diethyl ether (2 \times 5 mL). The crude product was purified via column chromatography on basic alumina, and eluted with dichloromethane to remove the impurities, then eluted with methanol. The resulting blue solution was concentrated and dissolved in 2 mL of hot CH₃CN, and then 2 mL of ether was added and the solution was allowed to cool to ambient temperature. The resulting solid was collected by filtration, washed with diethyl ether (2 \times 5 mL), and dried to give 0.15 g (78%) of **1-Te** as a dark green solid: mp $>260\text{ }^\circ\text{C}$. ^1H NMR (300 MHz, CD₃OD) δ 7.87 (d, 2H, $J = 3$ Hz), 7.60 (t, 3H, $J = 3$ Hz), 7.50 (d, 2H, $J = 10$ Hz), 7.30–7.27 (m, 2H), 6.89 (d \times d, 2H, $J = 3, 10$ Hz), 3.21 (s, 12H); ^{13}C NMR (125 MHz, CD₃OD) δ 165.1, 153.1, 141.5, 140.6, 139.3, 129.9, 129.6, 129.5, 122.4, 116.9, 115.8, 40.6; $\lambda_{\text{max}}(\text{CH}_2\text{Cl}_2)$ 601 nm (ϵ $8.1 \times 10^4\text{ M}^{-1}\text{ cm}^{-1}$); $\lambda_{\text{max}}(\text{H}_2\text{O})$ 597 nm (ϵ $7.4 \times 10^4\text{ M}^{-1}\text{ cm}^{-1}$); HRMS (ESI) m/z 457.0918 (calcd for C₂₃H₂₃N₂Te⁺; 457.0918). Anal. Calcd for C₂₃H₂₃N₂Te \cdot PF₆: C, 46.04; H, 3.86; N, 4.87. Found: C, 46.02; H, 3.85; N, 4.90.

2,7-Bis(dimethylamino)-9-(2-thienyl)telluroxanthylum Hexafluorophosphate (2-Te). *n*-Butyllithium (1.6 M in hexanes, 1.7 mL, 2.8 mmol) was added dropwise to a stirred solution of thiophene (0.21 mL, 2.8 mmol) and TMEDA (0.41 mL, 2.8 mmol) in 12 mL of anhydrous THF cooled to $-78\text{ }^\circ\text{C}$. This mixture was stirred for 1 h. A solution of telluroxanthone **4-Te** (100 mg, 0.254 mmol) dissolved in 4.0 mL of anhydrous THF was added dropwise, and

the resulting mixture was stirred 1 h at ambient temperature and was then heated at reflux for 0.5 h. The reaction mixture was treated with glacial acetic acid (0.5 mL) and poured into a 10% by wt solution of HPF₆ (100 mL). After the mixture was stirred for 1.0 h, the precipitate was collected and copiously washed with H₂O and ether. The crude product was recrystallized from equal volumes of CH₃CN/ether (2 \times) to give 91 mg (59%) of **2-Te** as dark green crystals, mp $>260\text{ }^\circ\text{C}$. ^1H NMR (500 MHz, CD₃OD) δ 8.08 (d, 2H, $J = 2.7$ Hz), 7.73 (d, 2H, $J = 9.7$ Hz), 7.65 (d \times d, 1H, $J = 1.5, 5.1$ Hz), 7.25 (d \times d \times d, 1H, $J = 1.5, 3.6, 5.1$ Hz), 7.15 (d \times d, 2H, $J = 1.5, 3.6$ Hz), 6.77 (d \times d, 2H, $J = 2.7, 9.7$ Hz), 3.23 (s, 12H); ^{13}C NMR (75 MHz, CD₃OD) δ 151.2, 150.6, 143.1, 135.6, 134.2, 130.8, 128.0, 126.7, 117.9, 112.8, 103.0, 58.5; $\lambda_{\text{max}}(\text{CH}_2\text{Cl}_2)$ 615 nm (ϵ $9.3 \times 10^4\text{ M}^{-1}\text{ cm}^{-1}$); HRMS (ESI) m/z 463.0488 (calcd for C₂₁H₂₁N₂S¹³⁰Te⁺: 463.0482). Anal. Calcd for C₂₁H₂₁N₂STe \cdot PF₆: C, 41.62; H, 3.49; N, 4.62. Found: C, 41.51; H, 3.50; N, 4.72.

2,7-Bis(dimethylamino)-9-(1-naphthyl)telluroxanthylum Hexafluorophosphate (5-Te). *sec*-Butyllithium (1.4 M in cyclohexanes, 400 μL , 0.51 mmol) was added dropwise to a stirred solution of TMEDA (80 μL , 0.51 mmol) and 1-bromonaphthalene (105 mg, 0.508 mmol) in 7 mL of anhydrous THF cooled to $-78\text{ }^\circ\text{C}$. The reaction mixture was then transferred via cannula into a solution of telluroxanthone **4-Te** (100 mg, 0.254 mmol) dissolved in 4.0 mL of anhydrous THF and slowly warmed to ambient temperature. The reaction mixture was treated with glacial acetic acid (0.5 mL) and poured into a 10% by wt solution of HPF₆ (100 mL). After the mixture was stirred for 1.0 h, the precipitate was collected and copiously washed with H₂O and ether. The crude product was recrystallized from equal volumes of CH₃CN/ether (2 \times) to give 91 mg (59%) of **5-Te** as dark green crystals, mp 195–196 $^\circ\text{C}$. ^1H NMR (400 MHz, CD₂Cl₂) δ 8.14 (d, 1H, $J = 8.4$ Hz), 8.06 (d, 1H, $J = 8.4$ Hz), 7.70 (m, 3H), 7.54 (t, 1H, $J = 7.6$ Hz), 7.43 (d, 2H, $J = 6.8$ Hz), 7.37 (t, 2H, $J = 8.4, 6.8$ Hz), 7.45 (d, 2H, $J = 10$ Hz), 6.67 (d \times d, 2H, $J = 2.4, 9.8$ Hz), 3.13 (s, 12H); ^{13}C NMR (75 MHz, CD₂Cl₂) δ 164.1, 153.2, 141.2, 138.6, 137.8, 137.4, 133.0, 130.0, 129.5, 128.3, 128.2, 127.7, 126.6, 126.3, 122.8, 116.8, 116.1, 40.8; $\lambda_{\text{max}}(\text{H}_2\text{O})$ 604 nm (ϵ $7.5 \times 10^4\text{ M}^{-1}\text{ cm}^{-1}$); $\lambda_{\text{max}}(\text{CH}_2\text{Cl}_2)$ 602 nm (ϵ $1.3 \times 10^5\text{ M}^{-1}\text{ cm}^{-1}$); HRMS (EI) m/z 507.1085 (calcd for C₂₇H₂₅N₂¹³⁰Te: 507.1080). Anal. Calcd for C₂₇H₂₅N₂Te \cdot PF₆: C, 49.89; H, 3.88; N, 4.31. Found: C, 50.23; H, 3.89; N, 4.37.

2,7-Bis(dimethylamino)-9-(5-carboxy-2-thienyl)telluroxanthylum Hexafluorophosphate (7-Te). *tert*-Butyllithium (1.7 M in pentane, 3.76 mL, 6.40 mmol) was added dropwise to a stirred solution of 5-bromothiophene-2-carboxylic acid (631 mg, 3.05 mmol) and TMEDA (117 μL , 0.762 mmol) in 30 mL of anhydrous THF cooled to $-78\text{ }^\circ\text{C}$. The reaction mixture was then transferred via cannula to a solution of telluroxanthone **4-Te** (300 mg, 0.762 mmol) dissolved in 9.0 mL of anhydrous THF. The resulting mixture was heated at 40 $^\circ\text{C}$ for 0.25 h and then cooled to ambient temperature. Glacial acetic acid (0.5 mL) was added, and the resulting mixture was poured into a 10% by wt solution of HPF₆ (100 mL). The precipitate was collected and washed with H₂O and ether after 1.0 h of stirring. The crude product was recrystallized from equal volumes of CH₃CN/ether (2 \times) to give 229 mg (46%) of **7-Te** as dark green crystals, mp 268–271 $^\circ\text{C}$. ^1H NMR (400 MHz, CD₃CN) δ 9.76 (br s, 1H), 7.89 (d, 1H, $J = 3.6$ Hz), 7.69 (d, 2H, $J = 2.4$ Hz), 7.65 (d, 2H, $J = 9.6$ Hz), 7.20 (d, 1H, $J = 3.6$ Hz), 6.87 (d \times d, 2H, $J = 2.4, 9.6$ Hz), 3.17 (s, 12H); ^{13}C NMR (125 MHz, CD₃CN) δ 162.6, 155.2, 153.0, 147.2, 140.6, 138.2, 136.5, 134.6, 131.9, 122.6, 116.9, 116.2, 40.9; $\lambda_{\text{max}}(\text{H}_2\text{O})$ 613 nm (ϵ $5.1 \times 10^4\text{ M}^{-1}\text{ cm}^{-1}$); $\lambda_{\text{max}}(\text{CH}_2\text{Cl}_2)$ 620 nm (ϵ $1.2 \times 10^5\text{ M}^{-1}\text{ cm}^{-1}$); HRMS (EI) m/z 507.0391 (calcd for C₂₂H₂₁N₂O₂S¹³⁰Te: 507.0386). Anal. Calcd for C₂₂H₂₁N₂O₂STe \cdot PF₆: C, 40.65; H, 3.26; N, 4.31. Found: C, 40.81; H, 3.32; N, 4.21.

2,7-Bis(dimethylamino)-9-(2-carboxyphenyl)telluroxanthylum Hexafluorophosphate (9-Te). *tert*-Butyllithium (1.6 M in

(32) Leonard, K. A.; Nelen, M. I.; Simard, T. P.; Davies, S. R.; Gollnick, S. O.; Oseroff, A. R.; Gibson, S. L.; Hilf, R.; Chen, L. B.; Detty, M. R. *J. Med. Chem.* **1999**, *42*, 3953–3964.

(33) Leonard, K. A.; Hall, J. P.; Nelen, M. I.; Davies, S. R.; Gollnick, S. O.; Oseroff, A. R.; Gibson, S. L.; Hilf, R.; Chen, L. B.; Detty, M. R. *J. Med. Chem.* **2000**, *43*, 4488–4498.

pentane, 2.67 mL, 4.28 mmol) was added dropwise to a stirred solution of 2-bromobenzoic acid (409 mg, 2.03 mmol) and TMEDA (84.4 μ L, 0.56 mmol) in 20 mL of anhydrous THF cooled to -78 °C. The reaction mixture was then transferred via cannula to a solution of telluroxanthone **4-Te** (200 mg, 0.51 mmol) dissolved in 6.0 mL of anhydrous THF, and the resulting mixture was heated at 40 °C for 15 min and then cooled to ambient temperature. Glacial acetic acid (0.5 mL) was added, and the resulting mixture was poured into a 10% by wt solution of HPF₆ (100 mL). After 1 h of stirring, the precipitate was collected by filtration and washed copiously with H₂O and ether. The crude product was recrystallized from equal volumes of CH₃CN/ether (2 \times) to give 292 mg (89%) of **9-Te** as bright green crystals, mp 291–292 °C. ¹H NMR (400 MHz, CD₃CN) δ 9.49 (s, broad, 1H), 8.26 (d \times d, 1H, J = 1.2, 7.6 Hz), 7.79 (t \times d, 1H, J = 1.2, 1.6, 7.6 Hz), 7.73 (t \times d, 1H, J = 1.2, 1.6, 7.6 Hz), 7.66 (d, 2H, J = 2.8 Hz), 7.28 (m, 3H), 6.76 (d \times d, 2H, J = 2.8, 10 Hz), 3.14 (s, 12H); ¹³C NMR (75 MHz, CD₃-CN) δ 166.6, 153.1, 142.3, 140.4, 138.2, 133.9, 132.4, 131.3, 130.5, 130.3, 122.4, 116.7, 115.9, 40.8; λ_{max} (H₂O) 595 nm (ϵ 7.1 \times 10⁴ M⁻¹ cm⁻¹); λ_{max} (CH₂Cl₂) 596 nm (ϵ 8.1 \times 10⁴ M⁻¹ cm⁻¹); HRMS (EI) m/z 501.0835 (calcd for C₂₄H₂₃N₂O₂¹³⁰Te: 501.0816). Anal. Calcd for C₂₄H₂₃N₂O₂Te \cdot PF₆: C, 44.76; H, 3.60; N, 4.35. Found: C, 44.42; H, 3.67; N, 4.24.

Julolidyl Telluroxanthylum Dye 3-Te. Telluroxanthone **6** (75 mg, 0.17 mmol) was dissolved in dry THF (10 mL). Phenylmagnesium bromide (1 M in THF, 1.7 mL, 1.7 mmol, 10 equiv) was added slowly, and the resulting mixture was heated at reflux for 1 h. The reaction mixture was cooled to ambient temperature and 10% aqueous HPF₆ was added slowly, and the resulting mixture was then poured into 400 mL of ice water. The resulting purple precipitate was collected by filtration, washed with ether (3 \times 25 mL), and recrystallized from CH₃CN/ether to give 98 mg (89%) of **3-Te** as a purple solid, 218–221 °C. ¹H NMR (500 MHz, CD₂-Cl₂) δ 7.59–7.56 (m, 3H), 7.49 (d, 1H, J = 2.5 Hz), 7.41 (d, 2H, J = 9.5 Hz), 7.26–7.24 (m, 2H), 7.19 (s, 1H), 6.71 (d \times d, 1H, J = 2.5, 9.5 Hz), 3.50 (t, 2H, J = 6.0 Hz), 3.47 (t, 2H, J = 6.0 Hz), 3.18 (s, 6H), 2.65–2.60 (m, 4H), 2.21 (q, 2H, J = 6.0 Hz), 1.95 (q, 2H, J = 6.0 Hz); ¹³C NMR (75.5 MHz, CD₂Cl₂) δ 163.3, 151.7, 148.9, 140.3, 140.1, 139.1, 137.9, 136.0, 129.6, 128.9, 128.7, 125.0, 122.99, 122.2, 122.02, 115.2, 114.5, 51.8, 51.2, 40.5, 30.8, 27.9, 20.9, 20.7; λ_{max} (MeOH) 604 nm (ϵ 1.17 \times 10⁵ M⁻¹ cm⁻¹); λ_{max} (CH₂Cl₂) 605 nm (ϵ 1.3 \times 10⁵ M⁻¹ cm⁻¹); HRMS (EI) m/z 509.1235 (calcd for C₂₇H₂₇N₂¹³⁰Te: 509.1231). Anal. Calcd for C₂₇H₂₇N₂Te \cdot PF₆: C, 49.73; H, 4.17; N, 4.30. Found: C, 50.01; H, 4.18; N, 4.30.

X-ray Diffraction Data. X-ray diffraction data on **1-Te** were collected at 90(1) K using a Bruker SMART APEX2 CCD diffractometer installed at a rotating anode source (Mo K α radiation, λ = 0.71073 Å) and equipped with an Oxford Cryosystems nitrogen gas-flow apparatus. The data were collected by the rotation method with 0.3° frame-width (ω scan) and 20 s exposure time per frame. Four sets of data (600 frames in each set) were collected for each compound, nominally covering complete reciprocal space. The data were integrated, scaled, sorted, and averaged using the SMART software package.³⁴ The structure was solved by direct methods using SHELXTL NT Version 6.14.³⁵ The structure was refined by full-matrix least-squares against F^2 .

Non-hydrogen atoms were refined anisotropically. Positions of hydrogen atoms were found by difference electron density Fourier synthesis. The CH₃ hydrogens were treated as part of idealized CH₃ groups with $U_{\text{iso}} = 1.5U_{\text{eq}}$, while the remainder of the hydrogen atoms were refined with the “riding” model with $U_{\text{iso}} = 1.2U_{\text{eq}}$.

(34) APEX2 and SAINT-Plus, Area Detector Control and Integration Software, Ver. 1.0-27; Bruker Analytical X-ray Systems: Madison, WI, 2004.

(35) SHELXTL, An Integrated System for Solving, Refining and Displaying Crystal Structures from Diffraction Data, Ver. 6.14; Bruker Analytical X-ray Systems: Madison, WI, 2003.

Crystallographic data are compiled in Table 1S in the Supporting Information. Atomic coordinates, anisotropic displacement parameters, bond lengths, and angles are given in Tables 2S–4S, respectively, in the Supporting Information.

Acquisition of ¹²⁵Te NMR Spectra. The NMR samples were prepared in CDCl₃ in 5-mm NMR tubes. The ¹²⁵Te NMR spectra were recorded on a Varian Inova-400 NMR spectrometer at 126.289 MHz and 55 °C. The spectral width for acquisition was set to 320 kHz with an acquisition time of 0.82 s. The data were collected for 16K transients, with a pulse width of 9 μ s and a relaxation delay of 3–4 s. The FIDs were transformed with an exponential line broadening function of 10–15 Hz. Samples were referenced relative to 2,6-diphenyltelluroxyran-4-one as an external standard with a chemical shift of δ 553 relative to Me₂Te (δ 0.0).³⁶

Theoretical Methods. Most of the density functional theory (DFT) and time-dependent DFT (TDDFT) computations were performed with Turbomole²⁷ quantum chemical software, version 5.7.1. Molecular geometries were fully optimized at the DFT level using the B3LYP hybrid functional^{37,38} and the default Ahlrichs SVP Gaussian-type basis set from the Turbomole basis set library. Response calculations were carried out with the hybrid functionals B3LYP, B3LYP (50% exact exchange) and the non-hybrid (“pure”) functional BLYP using the default Ahlrichs TZVP³⁹ basis. Because the lowest-energy excitations in the compounds studied here are valence excitations (π to π^*), the use of a diffuse basis did not yield any improvements over the results obtained with the polarized valence triple- ζ TZVP basis.

All optimizations and response calculations were performed with the conductor-like screening model (COSMO)⁴⁰ of solvation applied to the ground state. Solvent model parameters were configured using the cosmoprep program of the Turbomole package. For optimizations, the dielectric constant of the solvent was set to 4.8; the dielectric constants for response calculations were set to 1 (vacuo), 4.8 (chloroform), or 33.1 (methanol); all other solvent parameters were left at program default values. Default optimized COSMO atomic radii were used. Orbital visualizations were done using gOpenMol.⁴¹ The natural bond order (NBO)⁴² analyses were carried out using the NBO version 3 code implemented in Gaussian 03 (G03).⁴³ In the G03 computations, the same basis sets and density functionals were applied as in the computations with the Turbomole code.

(36) Dety, M. R.; Lenhart, W. C.; Gassman, P. G.; Callstrom, M. R. *Organometallics* **1989**, *8*, 861–867.

(37) Becke, A. D. *J. Chem. Phys.* **1993**, *98*, 5648–5652.

(38) Hertwig, R. H.; Koch, W. *Chem. Phys. Lett.* **1997**, *268*, 345–351.

(39) Eichkorn, K.; Weigand, F.; Treutler, O.; Ahlrichs, R. *Theor. Chem Acc.* **1997**, *97*, 119.

(40) Schafer, A.; Klamt, A.; Sattel, D.; Lohrenz, J. C. W.; Eckert, F. *Phys. Chem. Chem. Phys.* **2000**, *2*, 2187.

(41) Laaksonen, L. *J. Mol. Graphics* **1992**, *10*, 33. Bergman, D. L.; Laaksonen, L.; Laaksonen, A. *J. Mol. Graphics Modell.* **1997**, *15*, 301.

(42) Weinhold, F. Natural bond orbital methods. In *Encyclopedia of computational chemistry*; von Rague Schleyer, P., Ed.; John Wiley & Sons: Chichester, 1998; pp 1792–1811.

(43) Frisch, M. J.; Trucks, G. W.; Schlegel, H. B.; Scuseria, G. E.; Robb, M. A.; Cheeseman, J. R.; Montgomery, J. A., Jr.; Vreven, T.; Kudin, K. N.; Burant, J. C.; Millam, J. M.; Iyengar, S. S.; Tomasi, J.; Barone, V.; Mennucci, B.; Cossi, M.; Scalmani, G.; Rega, N.; Petersson, G. A.; Nakatsuji, H.; Hada, M.; Ehara, M.; Toyota, K.; Fukuda, R.; Hasegawa, J.; Ishida, M.; Nakajima, T.; Honda, Y.; Kitao, O.; Nakai, H.; Klene, M.; Li, X.; Knox, J. E.; Hratchian, H. P.; Cross, J. B.; Bakken, V.; Adamo, C.; Jaramillo, J.; Gomperts, R.; Stratmann, R. E.; Yazyev, O.; Austin, A. J.; Cammi, R.; Pomelli, C.; Ochterski, J. W.; Ayala, P. Y.; Morokuma, K.; Voth, G. A.; Salvador, P.; Dannenberg, J. J.; Zakrzewski, V. G.; Dapprich, S.; Daniels, A. D.; Strain, M. C.; Farkas, O.; Malick, D. K.; Rabuck, A. D.; Raghavachari, K.; Foresman, J. B.; Ortiz, J. V.; Cui, Q.; Baboul, A. G.; Clifford, S.; Cioslowski, J.; Stefanov, B. B.; Liu, G.; Liashenko, A.; Piskorz, P.; Komaromi, I.; Martin, R. L.; Fox, D. J.; Keith, T.; Al-Laham, M. A.; Peng, C. Y.; Nanayakkara, A.; Challacombe, M.; Gill, P. M. W.; Johnson, B.; Chen, W.; Wong, M. W.; Gonzalez, C.; Pople, J. A. *Gaussian 03*, revision C2; Gaussian, Inc.: Pittsburgh, PA.

Acknowledgment. This research was supported in part by the Department of Defense [Breast Cancer Research Program] (Award No. W81XWH-04-1-0368) and by the Office of Naval Research (Award No. N0014-02-1-0836). Views and opinions of and endorsements by the authors do not reflect those of the U.S. Army or the Department of Defense. We acknowledge support from the Center of Computational Research at SUNY Buffalo. J.A. is grateful for financial support from the CAREER program of the National Science Foundation (grant no. CHE-0447321). B.C. thanks Matthew Kundrat for help with the computations.

Supporting Information Available: General experimental details, synthetic procedures for the preparation of **2-O**, **9-S**, and

9-Se, tables of crystallographic data, atomic coordinates and equivalent isotropic displacement parameters, anisotropic displacement parameters, and bond lengths and angles for **1-Te**, visualizations of the HOMOs and LUMOs and figures showing theoretical versus experimental excitation energies with B3LYP and BLYP functionals for the dye series **1-E** and **2-E**, figures showing the optimized geometry of **1-Te** and the resulting **1-Te(Se)** and **1-Te(S)** structures, and ^{125}Te NMR spectra for **1-Te**, **2-Te**, **3-Te**, **4-Te**, **5-Te**, and **10-Te**. This material is available free of charge via the Internet at <http://pubs.acs.org>.

OM700846M